AIP | The Journal of Chemical Physics

Characterization of porosity in vapor-deposited amorphous solid water from methane adsorption

U. Raut, M. Famá, B. D. Teolis, and R. A. Baragiola

Citation: The Journal of Chemical Physics **127**, 204713 (2007); doi: 10.1063/1.2796166
View online: http://dx.doi.org/10.1063/1.2796166
View Table of Contents: http://scitation.aip.org/content/aip/journal/jcp/127/20?ver=pdfcov
Published by the AIP Publishing

Characterization of porosity in vapor-deposited amorphous solid water from methane adsorption

U. Raut,[a] M. Famá, B. D. Teolis, and R. A. Baragiola
Laboratory of Atomic and Surface Physics, University of Virginia, Charlottesville, Virginia 22904, USA

(Received 7 August 2007; accepted 18 September 2007; published online 30 November 2007)

We have characterized the porosity of vapor-deposited amorphous solid water (ice) films deposited at 30–40 K using several complementary techniques such as quartz crystal microgravimetry, UV-visible interferometry, and infrared reflectance spectrometry in tandem with methane adsorption. The results, inferred from the gas adsorption isotherms, reveal the existence of microporosity in all vapor-deposited films condensed from both diffuse and collimated water vapor sources. Films deposited from a diffuse source show a step in the isotherms and much less adsorption at low pressures than films deposited from a collimated source with the difference increasing with film thickness. Ice films deposited from a collimated vapor source at 77° incidence are mesoporous, in addition to having micropores. Remarkably, mesoporosity is retained upon warming to temperatures as high as 140 K where the ice crystallized. The binding energy distribution for methane adsorption in the micropores of ice films deposited from a collimated source peaks at ~0.083 eV for deposition at normal incidence and at ~0.077 eV for deposition at >45° incidence. For microporous ice, the intensity of the infrared bands due to methane molecules on dangling OH bonds on pore surfaces increases linearly with methane uptake, up to saturation adsorption. This shows that the multilayer condensation of methane does not occur inside the micropores. Rather, filling of the core volume results from coating the pore walls with the first layer of methane, indicating pore widths below a few molecular diameters. For ice deposited at 77° incidence, the increase in intensity of the dangling bond absorptions modified by methane adsorption departs from linearity at large uptakes. © *2007 American Institute of Physics*.
[DOI: 10.1063/1.2796166]

I. INTRODUCTION

Vapor-deposited amorphous ice [also called amorphous solid water (ASW)] continues to attract much fundamental research[1] due to its occurrence in astronomical environments such as icy satellites, comets, planetary rings,[2] and interstellar grains.[3] Studies of gas adsorption on vapor-deposited amorphous ice have revealed that the amount of gas uptake is consistent with microporosity (defined as pore width <2 nm),[4] and large specific surface areas of up to hundreds of m^2/g. Recent experimental studies and related ballistic deposition modeling of condensation of ice films have confirmed the prediction[5] that the porosity of vapor-deposited ice depends on deposition angle.[6,7] Yet important parameters such as pore shape and structure, distributions of adsorption energies, and pore size remain largely unknown.

To cast light on these fundamental questions, we have measured methane adsorption isotherms on vapor-deposited ice films condensed from collimated and diffuse background sources of water vapor at 30 and 40 K in ultrahigh vacuum, at background pressures many orders of magnitude smaller than the vapor pressure of methane at 40 K. This enabled us to study the equilibrated methane uptake by amorphous ice over a wide pressure range spanning five orders of magnitude. We also characterized the porosity of the ice films through infrared spectroscopy of OH dangling bond (DB) absorption bands due to water molecules on the internal surface of the pore walls.[8] We used these complementary techniques to study the occurrence of microporosity and mesoporosity under different experimental conditions and to derive information on the binding energy distribution of the adsorption sites.

II. EXPERIMENTAL METHODS

All experiments were performed in ultrahigh vacuum conditions (base pressure of $\sim 10^{-10}$ Torr). Ice films were deposited from a collimated vapor flux at different incidence angles and, in some cases, from a diffuse background flux onto the gold mirror surface of a quartz crystal microbalance[9] cooled to 30 or 40 K. The mass per unit area of the films and its increase due to methane adsorption were measured with the microbalance, and were used to derive column densities by dividing by the appropriate molecular masses. The microbalance was surrounded by a heat shield cooled to ~90 K to reduce the radiative heat transfer from the surrounding room temperature chamber walls and provide additional pumping. Openings in the heat shield allow film deposition and optical measurements. In experiments where ice films were deposited from a background vapor source, the substrate faced away (~180°) from the doser and the heat shield was removed to avoid partial collimation. From here on, we will refer to the films deposited from col-

[a]Electronic mail: ur5n@virginia.edu.

limated flux by their deposition angle (for instance, 45° film), and the background deposited films will be referred to as background deposited ice (BDI).

We grew ice films with column densities of 1.02×10^{18} molecules/cm^2 (and, in one instance, 1.02×10^{17} molecules/cm^2). The film thickness d and refractive index n were derived by fitting the Fresnel equations to the interference pattern in the optical reflectance in the 250–600 nm (Refs. 5 and 10) range. The ice density ρ was calculated from the ratio of the mass column density of the film obtained from the microbalance to the film thickness. Using 0.94 g/cm^3 for density of compact ice ρ_c,[11] we obtained the porosity ($\Phi = 1 - \rho/\rho_c$) of the ice films, and found it to increase with deposition angle as in earlier studies.[6] The films were characterized by specular infrared reflectance spectroscopy (35° incidence angle) at 2 cm^{-1} resolution with a Nicolet 670 Fourier transform infrared spectrometer thoroughly purged with dry air. The infrared spectra were expressed in optical depth units, $-\ln(\mathbf{R}/\mathbf{R}_0)$, where $\mathbf{R}$ is the reflectance of the film-substrate system and $\mathbf{R}_0$ that of the bare gold substrate. The band areas of the DB absorption features were obtained after subtracting a baseline fit to the continuum absorption.

Following film deposition, we admitted methane gas (99.999% pure) into the vacuum chamber and measured its uptake θ (molecules/cm^2) at 20 and 40 K from the change in mass of the films measured with the microbalance. At 20 K, the rate of CH_4 desorption from the ice is negligible, and thus θ increased with time at a constant rate when the ice was exposed to a constant CH_4 pressure $P(\sim 5 \times 10^{-8}$ Torr), stopping only when the methane flow was interrupted. In contrast, at 40 K the rate of CH_4 desorption was significant and the uptake was determined by the competition between desorption and adsorption. As a result, θ initially increased linearly with time after methane was admitted into the chamber, and asymptotically approached a constant level at which the adsorption and desorption rates were equal. Subsequent increases in pressure disturbed the equilibrium, causing θ to increase to a new plateau. Thus, we increased the pressure in steps, recording several saturation values of θ at different pressures up to a critical pressure P_{max}. Above P_{max} continuous condensation of methane occurs on top of the ice films. We note that since the gas and solid phases of methane are at different temperatures, P_{max} is not the saturation vapor pressure P_0 but $P_0(T_{rt}/T)^{0.5}$, with T and T_{rt} being the ice and room temperature. During methane adsorption, we also measured the film thickness by fitting Fresnel equations to the optical reflectance.

III. RESULTS AND DISCUSSION

Figure 1 shows infrared absorption spectra in the region of the dangling OH bands (~2.7 μm) of amorphous ice and the effect of methane absorption, for films condensed under different deposition conditions. These bands, which are usually insignificant in compact ice, are enhanced because of the large internal surface area in porous ASW films.[1] The infrared spectra in the top panel of the figure show the absorption features, DB1 (3720 cm^{-1}) and DB2 (3696 cm^{-1}), assigned

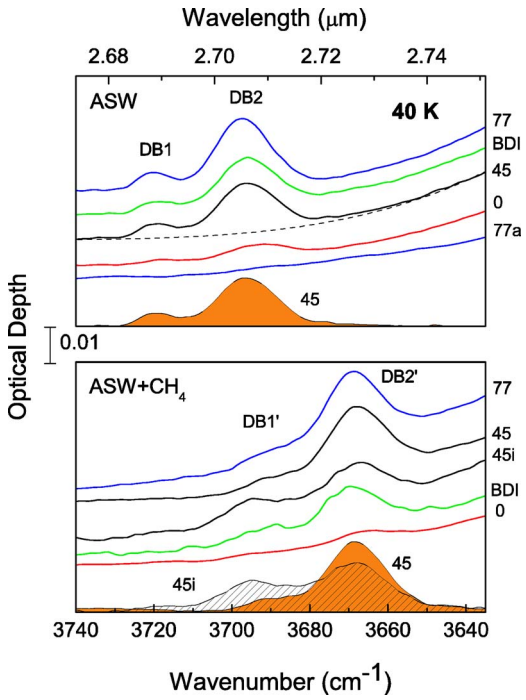

FIG. 1. (Color online) Comparison of dangling bond (DB1 and DB2) features of ice films deposited at 40 K with column density of 1.02×10^{18} H_2O/cm^2. The spectra have been vertically shifted for clarity. The numbers 0, 45, and 77 refer to the deposition angles in degrees (77a is for the 77° film after warming to 140 K). BDI denotes background deposited ice. Top panel: ASW before methane exposure. The shaded region is the DB features of the 45° film after subtraction of the continuum baseline (dashed line). Bottom panel: ASW after methane uptake. The gas uptakes in units of 10^{15} CH_4/cm^2 are 168 (45°), 109 (BDI), 38 (0°), and 402 (77°) corresponding to maximum uptake. The curve labeled 45i is for a 45° film with an intermediate uptake of 90×10^{15} CH_4/cm^2. The shaded bottom curves are for the corresponding spectra after the appropriate baseline subtraction.

to O–H vibrations of doubly coordinated and triply coordinated surface water molecules, respectively.[12] The bottom panel of Fig. 1 shows the changes in the dangling bond features that occur due to methane adsorption at 40 K. The vibrational frequencies decrease when foreign molecules such as methane attach to the dangling bonds, and as a result the DB1 and DB2 features disappear and new features DB1′ and DB2′ emerge at 3691 and 3669 cm^{-1}, as seen previously.[13,14] This shift in the frequencies of the DB features with increasing CH_4 uptake is illustrated by the spectra denoted by 45i and 45 in the bottom panel of Fig. 1. Note that the DB1′ feature occurs at approximately the same frequency as the DB2 band for ice without adsorbed gas. The shaded regions in Fig. 1 show the DB features (with and without CH_4) of the film deposited at 45° incidence after subtraction of the continuum baseline indicated by the black dashed line. The integrated band areas of both dangling bond features of the ice films, deposited at different incidence angles (0°, 45°, and 77°) at 40 K prior to methane exposure, increase with film porosity (Table I). We note that, in all the experiments reported here, there is no indication of unshifted dangling bonds at high gas uptake. This indicates that the number of closed or inaccessible pores is insignificant.

Figure 2 shows the adsorption isotherms, the dependence of the CH_4 uptake on relative pressure $p = P/P_{max}$ at 40 K for ice films deposited under different deposition conditions.

TABLE I. Comparison of different properties observed for vapor-deposited ice films deposited at 40 K with column density of 1.02×10^{18} H_2O/cm^2.

Angle of incidence	0°	45°	77°	77° annealed at 140 K	Diffuse (BDI)
DB band area without CH_4 (cm^{-1})	0.068±0.001	0.252±0.002	0.381±0.003	<0.008	0.248±0.002
Porosity	0.08±0.01	0.22±0.07	0.40±0.06	0.13±0.02	0.21±0.04
Maximum methane uptake ($10^{15}/cm^2$)	42±2	169±3	407±4	85±2	
Film thickness (nm)	354±10	417±6	540±5	376±7	412±5
Average methane density in pores (g/cm^3)	0.39±0.06	0.48±0.02	0.50±0.03	0.46±0.03	
Type of porosity	micro	micro	micro/meso	meso	micro
Freundlich exponent	0.19±0.01	0.20±0.04	0.20±0.01	~ 1	0.30±0.03
Dubinin-Astakhov exponent	1.89±0.05	2.04±0.07	2.00±0.06		
Most probable binding energy (eV)	0.083	0.077	0.077		

Each data point represents the equilibrium between CH_4 adsorption and desorption. At low pressures, the equilibrium is reached at adsorption sites of high binding energies, and, as pressure increases, sites of increasingly lower binding energy are populated until all sites are filled. We find that the isotherms of 45° and 0° films have the distinct shape of a *Type I* isotherm,[15–17] i.e., they rise sharply at low pressures ($p<0.1$) and reach a plateau where all adsorption sites are filled. The *Type I* shape for the two films indicates a fully microporous film.[16] Note that the maximum uptake measured at P_{max} for these two films is not proportional to the film porosity, which suggests that the average density of methane inside the pores is different in these cases. Table I also gives the average density of methane in the micropores obtained by dividing the maximum mass uptake by the pore volume.

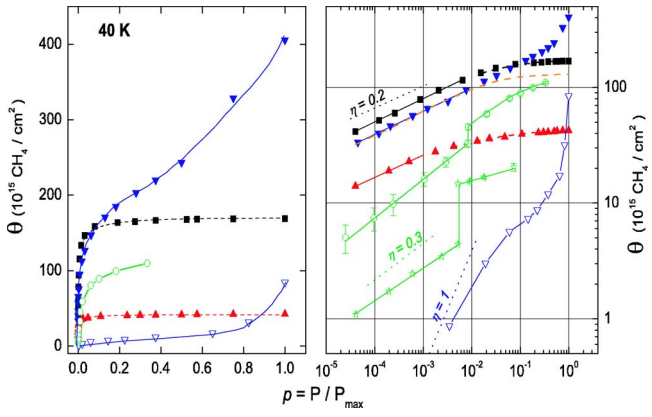

FIG. 2. (Color online) CH_4 uptake θ vs pressure for different ice films at 40 K: left (linear scale) and right (logarithmic scale). The angles of incidence of films deposited with a directional water flux are (■) 45° black square, (▲) 0° red triangle, and (▼) 77° blue inverted triangle. The orange dashed line (---) is the 45° isotherm scaled to match the 77° isotherm in the $p<10^{-2}$ regime. (▽): 77° film warmed to 140 K. The CH_4 uptake for background vapor deposition is shown for films with column densities of (○) 1.02×10^{18} H_2O/cm^2 and (☆) 1.02×10^{17} H_2O/cm^2. The solid unbroken lines in the linear plot are guides to the eye. The dashed lines in the linear plot are fits of the Dubinin-Astakhov equation in the high pressure regime ($p>10^{-2}$). The solid lines in the logarithmic plot are fits of the Freundlich equations in the low pressure regime ($p<10^{-3}$). The dotted lines represent different values of the Freundlich exponent η.

The values obtained are smaller than the value of 0.52 g/cm^3 for solid methane.[18]

The shape of the adsorption isotherm is drastically different for the film deposited at an oblique incidence of 77°. The plateau observed in the isotherms of the 0° and 45° films is replaced by a steady increase in uptake up to P_{max}. This second increase in uptake is typical of a type II isotherm, which is observed in mesoporous solids having larger pores measuring 2–50 nm in width.[15] The formation of larger pores at large incidence angles is consistent with the results of ballistic deposition simulations, suggesting the importance of shadowing of incoming molecules by protruding surface structures.[19] The increase in gas uptake with increasing deposition angle is consistent with previous studies using nitrogen.[6]

Interestingly, while the maximum gas uptake of the 77° film is more than twice that of the 45° film, for $p<0.01$ the ratio is only 0.81. This difference is more easily visualized when the isotherms are plotted in logarithmic scale as shown in right side of Fig. 1. The similar shape of the isotherms of the 45° and the 77° films at $p<0.01$ indicates that, in addition to mesopores, the 77° film contains micropores. To separate adsorption due to micropores from the total adsorption, we scale the 45° isotherm to match the 77° isotherm at low pressures. The scaled isotherm shows an uptake of 130×10^{15} CH_4/cm^2 at $p=1$. The maximum uptake of 407×10^{15} CH_4/cm^2 for the 77° film therefore implies that its mesopores can adsorb up to 277×10^{15} CH_4/cm^2.

Crystallization resulted when the 77° film was warmed to 140 K, as revealed by the sharpening of the 3 μm OH-stretch band[1,20] and the emergence of the weak 1.65 μm band.[21] Remarkably, the crystalline ice retains porosity ($\Phi=0.13$, i.e., roughly 1/3 of the original amount). However, while the film is still porous, the dangling bond infrared absorptions have disappeared (Fig. 1). Additionally, warming resulted in the release of the adsorbed methane; infrared spectroscopy of the methane bands showed that less than 5×10^{14} CH_4/cm^2 remained trapped beyond 65 K. After cooling the annealed film back to 40 K, we measured a new adsorption isotherm. We found that the methane uptake was

drastically lower than before warming and that it increased linearly with pressure at low p (Fig. 2). The surge in the uptake when p exceeds 0.1 shows that the residual porosity ($\Phi=0.13$) is due to mesopores, thus indicating that such pores are much less susceptible to collapse during warming than the smaller micropores.

We note that our previous study on compaction of microporous ASW by ion irradiation[14] revealed that ice could remain porous and not have dangling bond features when irradiated with energetic particles. Here, we find another instance where ice remains porous but lack in dangling bond features. Therefore, the absence of the dangling bond features in the infrared spectra of laboratory or extraterrestrial ices does not necessarily guarantee compact ice.

The isotherm of the BDI film is remarkably different from those of the films deposited from a collimated water flux. While the BDI film has a porosity ($\Phi=0.21$) and dangling bond features similar to those of the 45° film (Fig. 1), its CH_4 uptake is nearly an order of magnitude smaller at the lowest pressures ($p\sim 4\times 10^{-5}$). Since there is no indication of unshifted dangling bonds at high uptake (Fig. 1), the number of inaccessible pores is insignificant. Therefore, the uptake is reduced because the majority of the micropores is large (with small binding energy) compared with the case of the 45° film. Remarkably, the isotherm of the BDI film exhibits a step at $p\sim 0.01$, where, at a constant pressure and after an initial saturation, the uptake increases very slowly with time until a second higher saturation value is reached. Steps in adsorption isotherms have been previously observed in other adsorption studies[22] and are thought to indicate a phase transition of the two-dimensional adsorbed layer.[23] Unfortunately, our current experimental setup does not allow us to measure the isotherms with decreasing pressures to determine if the transition is irreversible or if there is hysteresis. We also recorded CH_4 isotherm in another BDI film with ten times smaller column density than that of the other films (1.02×10^{17} H_2O/cm^2). Remarkably, the uptake at low pressures was only approximately five times less. Therefore, the pore structure of the BDI films also depends on film thickness. Figure 2 shows that the size of the step in the isotherm is about the same (but relatively larger) in the thinner BDI film.

The three films deposited from a collimated vapor at different incidence angles (0°, 45°, and 77°) have the same shape in the low pressure regime ($p<10^{-3}$) and their isotherms can be fitted with the empirical Freundlich equation, $\theta=\beta p^{\eta}$, where β is a constant and η is the Freundlich exponent,[15,22] a measure of the heterogeneity of adsorption energies.[22] Although the physics behind the Freundlich equation has not been elucidated, we report here the values of exponents from fits to the data for possible comparisons with other microporous materials. We obtain $\eta\sim 0.2$ for all three films deposited from collimated vapor flux at different incidence (0°, 45°, and 77°), but ~0.3 for the BDI films. In the higher pressure regime, we fit the isotherms with the Dubinin-Astakhov equation which, despite being also empirical, is widely used to describe adsorption of gases in a variety of microporous solids.[15] It reads

$$\frac{\theta}{\theta_{\max}}=\exp\left(\frac{kT}{\varepsilon_c}\ln p\right)^N, \tag{1}$$

where $\theta/\theta_{\max}$ is the fractional uptake, k is Boltzmann's constant, T is the temperature, p is the relative pressure, ε_c is a characteristic adsorption energy, and N is a heterogeneity parameter.[24] The fits of the equation at high pressures, also included in Fig. 2 for ice films deposited from collimated vapor, yield $N\sim 2$, in the range of reported values.[22]

The distribution of adsorption energies ε_i in microporous solids is usually associated with a distribution in pore size, which influences the degree of overlapping of the interaction potentials from opposite pore walls, and consequently the depth of the adsorption potential well.[15] Beside the dispersion in pore size, the microscopic roughness of the pore wall can also contribute to energetic heterogeneity. To obtain the adsorption energy distributions from the experimental isotherms, we apply the condensation approximation[25] to map the relative pressure scale $P/P_{\max}$ into an energy scale. Since molecules diffuse fast in the pores, as will be shown later when reporting experiments at 20 K, we assume that absorption obeys Henry's law locally, in which the probability that an incoming molecule finds an empty site is independent of the fractional coverage ϑ and zero above $\vartheta=1$ (full coverage). In each ensemble of sites with binding energy ε, ϑ is given by

$$\vartheta(P,\varepsilon,T)=KP\exp(\varepsilon/kT), \tag{2}$$

up to $\vartheta=1$. K is a constant for a given gas-ice combination at a fixed temperature T, and k is the Boltzmann constant. Since, in practice, $\varepsilon\gg kt$, the steep rise in the exponential allows approximating Eq. (2) by a step function of energy. This is the condensation approximation, where, at a given P and T, all sites with binding energy $\geqslant\varepsilon_i$ are completely filled ($\vartheta=1$) and all with lower energy are unoccupied ($\vartheta=0$). For an arbitrary value of ϑ_i

$$KP=\vartheta_i\exp(-\varepsilon_i/kT). \tag{3}$$

In the limit of $P_{\max}$, adsorption occurs on sites with the lowest binding energy ε_o. Thus,

$$KP_{\max}=\vartheta_i\exp(-\varepsilon_o/kT). \tag{4}$$

Dividing Eq. (2) by Eq. (3) yields

$$\varepsilon_i=\varepsilon_o-kT\ln(P/P_{\max}). \tag{5}$$

We also note that Eq. (5) also holds for any monolayer adsorption law, such as Langmuir, as long as it applies equally for sites of different binding energy. In the top panel of Fig. 3 we plot the integrated CH_4 uptake in pores with adsorption energies above energy ε_i using Eq. (5) with $\varepsilon_o\approx 0.06$ eV, the binding energy measured for methane on a flat water ice surface.[26] The numerical differentiation of the integral uptake yields $d\theta/d\varepsilon$, the distribution of the CH_4 uptake among sites of different adsorption energies shown in the bottom panel. The peak of the adsorption energy distribution ε_p of the 0° film is at ~0.083 eV, while the ε_p for 45° film is at 0.077 eV, the difference being outside statistical

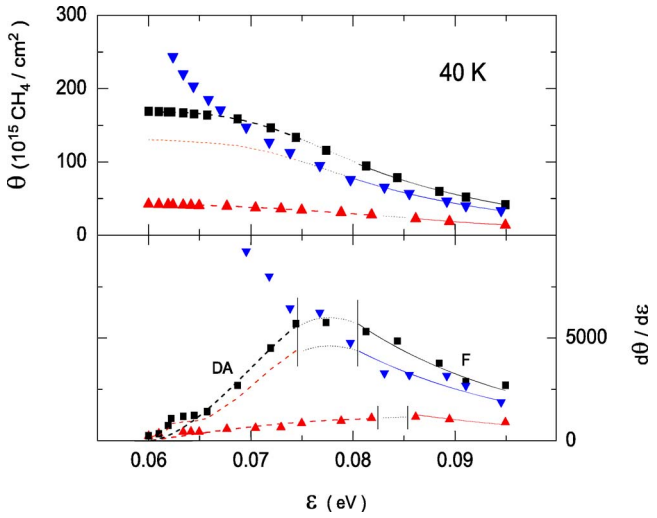

FIG. 3. (Color online) Top panel: The integral methane uptake in the micropores with binding energies higher than ε_i for ice films deposited from a collimated vapor beam at 0° (▲) red triangle, 45° (■) black box, and 77° (▼) blue inverted triangle incidence angles. The orange dashed line shows the uptake in the micropores of the film deposited at 77° incidence and is obtained by scaling the isotherm of the 45° film (Fig. 2). The fits of the Dubinin-Astakhov (DA) (dashed lines) and Freundlich (F) equations (solid lines) are also shown. Bottom panel: The distribution of methane uptake in pores with different binding energies (e_i) obtained from numerical differentiation of the curves in the top panel. The vertical lines delimit the region where neither the DA nor the F equations are valid.

errors. We also show the results derived from fitting the Dubinin-Astakhov and the Freundlich equations to the relevant pressure regimes.

We now analyze the infrared spectra and consider the integrated area of the dangling bonds to be a measure of the surface area of the pores. Figure 4 (bottom) shows that the

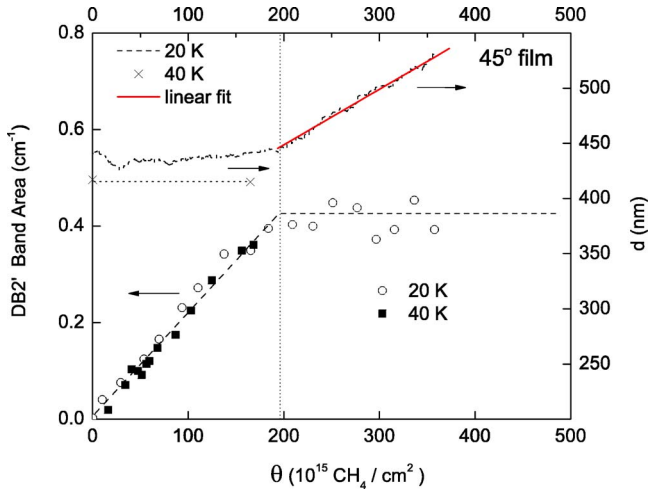

FIG. 4. (Color online) Increase in the DB2′ band area with CH_4 uptake (θ) at 20 and 40 K. The dashed line is a guide to the eye and the vertical dotted black line indicates the uptake required for complete filling of the pores with methane in the 20 K film. The top part of the graph shows the change in thickness of the ice films with θ at 20 K (black line) and 40 K (+) measured by UV-vis interferometry. At 20 K, the methane pressure ($\sim 10^{-8}$ Torr) exceeds the vapor pressure ($\sim 10^{-13}$ Torr) causing methane to condense above the external ice surface, thereby increasing the film thickness but only after the pores are saturated with gas. Note that the DB band area remains unchanged when methane condenses to form an external overlayer. The ice films were deposited at 45° incidence.

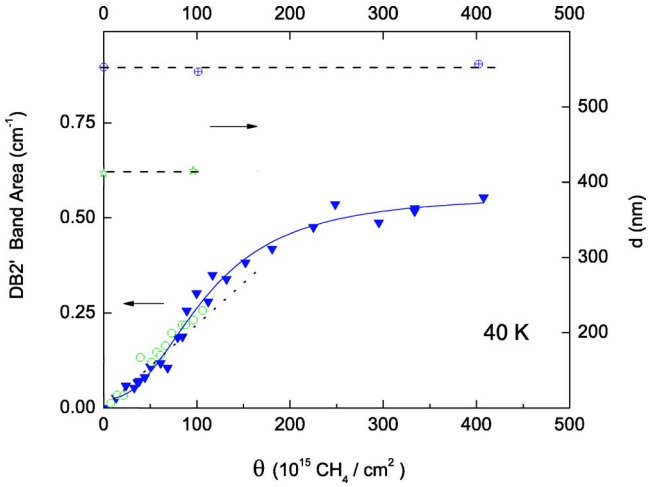

FIG. 5. (Color online) Increase in the DB2′ band area with CH_4 uptake (θ) at 40 K for a 77° film (inverted triangles) and a background-deposited ice film (open circles), compared to the data shown in Fig. 4 for a 45° film (···). The lines are to guide the eye. The data in the top of the graph and the horizontal lines show that the film thickness for the BDI film (stars) and the 77° film (⊗) remain constant up to the saturation uptake (at P_{max}). All films have 10^{18} H_2O/cm^2.

results for a film with a porosity $\Phi=0.26$, deposited at 45° incidence at 30 K, warmed to 40 K, then exposed to methane at 20 K. The DB2′ area increased linearly with CH_4 uptake and saturated when θ exceeded what we call $\theta_c \sim 200 \times 10^{15}$ CH_4/cm^2. Remarkably, the total film thickness remained constant at ~440 nm until θ exceeded θ_c, implying that the adsorbed methane does not accumulate as a layer external to the film, but rather diffuses into the internal pore volume. Above θ_c the film thickness increases linearly with uptake and the inverse of the slope gives a density of 0.52 g/cm^3 for solid methane, equal to published values.[18,27] We calculate the average methane density inside the pores of the film at 20 K to be 0.47 ± 0.03 g/cm^3. The linear dependence of the DB2′ area on CH_4 uptake and the constancy of the film thickness with CH_4 adsorption is also seen for a film deposited at 45° but at 40 K with $\Phi=0.22$.

Earlier we mentioned that the dispersion in the pore width is usually assumed to be the main source of the energetic heterogeneity in the microporous films, i.e. small pores are the adsorption sites with high binding energy and larger pores are the sites with low binding energy. As discussed before, an increase in pressure leads to CH_4 adsorption in pores with lower binding energies, i.e., larger pores. In pores smaller than three molecular diameters in width all the adsorbed molecules coat the pore surface and the number of dangling bonds modified will be proportional to the amount of gas adsorbed. On the other hand, in larger pores, adsorbed molecules could occupy the core volume of the pores without contributing to shifted dangling bond bands. Therefore, the observed linear dependence of DB2′ areas with methane uptake (Fig. 4) implies that, within errors, all adsorbed molecules fill the pores by coating their surfaces. In other words, the pore widths in our fully microporous ice must not exceed three molecular diameters. The same behavior is observed in the BDI films (Fig. 5), in spite of the presence of a step in their adsorption isotherms. Interestingly, the DB2′ band area

versus θ of the 77° film deviated by about 10%–15% from the other cases at low θ and becomes strongly nonlinear at large uptakes where the mesopores can be filled by multilayer adsorption. The thickness of the BDI and 77° films remained constant up to the maximum uptake.

IV. SUMMARY AND CONCLUSIONS

We have presented a detailed study of porosity-related properties of ASW films deposited at 30–40 K using the complementary techniques of microbalance gravimetry, UV-visible spectroscopic interferometry, and infrared spectroscopy. Table I shows a comparison of the different properties of vapor-deposited ice films condensed from collimated and diffuse background sources. Our major findings are as follows:

(i) All amorphous ice films deposited at 30–40 K, irrespective of their deposition method, have micropores as deposited.
(ii) Ice films deposited at 77° incidence from a collimated vapor source develop a dual pore structure, having both micro- and mesopores. A brief annealing at 140 K crystallizes the ice and destroys the microporosity, but remarkably, some mesopores remain.
(iii) The similar shape (same Freundlich exponent) of the adsorption isotherms at low pressure for the films deposited from a collimated vapor at different angles indicates similar microstructures responsible for high binding energies, even though the total porosity depends strongly on deposition angle.
(iv) Films deposited from a diffuse background vapor source have isotherms with a larger Freundlich exponent and a step, suggesting that their micropores are different from those in films deposited from a collimated vapor source.
(v) The ice films deposited from a diffuse source adsorb much less gas per unit pore volume than the films deposited unidirectionally, and show a step in the adsorption isotherms.
(vi) The micropores are narrow (less than three molecular diameters wide) since there is only evidence for monolayer adsorption.

The different pore structures found in this research can occur in astronomical environments, depending on local deposition conditions, and affect the gas trapping. This can have consequences, for instance, for determining properties of comets.

ACKNOWLEDGMENTS

This research was supported by the NASA Origins of the Solar System and NSF Astronomy programs.

[1] R. A. Baragiola, in *Water In Confining Geometries*, edited by J. P. Devlin and V. Buch (Springer, Berlin, 2003).
[2] B. Schmitt, C. de Bergh, and M. Festou, *Solar System Ices* (Kluwer Academic, Dordrecht, 1998).
[3] D. C. B. Whittet, W. A. Schutte, A. Tielens, A. C. A. Boogert, T. de Graauw, P. Ehrenfreund, P. A. Gerakines, F. P. Helmich, T. Prusti, and E. F. van Dishoeck, Astron. Astrophys. **315**, L357 (1996); P. T. O'Neill and D. A. Williams, Astrophys. Space Sci. **266**, 539 (1999); P. Ehrenfreund and W. A. Schutte, Adv. Space Res. **25**, 2177 (2000).
[4] E. Mayer and R. Pletzer, Nature (London) **319**, 298 (1986); C. Manca, P. Roubin, and C. Martin, Chem. Phys. Lett. **330**, 21 (2000); C. Martin, C. Manca, and P. Roubin, Surf. Sci. **502**, 280 (2002); B. Schmitt, J. Ocampo, and J. Klinger, J. Phys. (Paris) **48**, 519 (1987); P. Ayotte, R. S. Smith, K. P. Stevenson, Z. Dohnalek, G. A. Kimmel, and B. D. Kay, J. Geophys. Res. **106**, 33387 (2001).
[5] M. S. Westley, G. A. Baratta, and R. A. Baragiola, J. Chem. Phys. **108**, 3321 (1998).
[6] K. P. Stevenson, G. A. Kimmel, Z. Dohnalek, R. S. Smith, and B. D. Kay, Science **283**, 1505 (1999).
[7] Z. Dohnalek, G. A. Kimmel, P. Ayotte, R. S. Smith, and B. D. Kay, J. Chem. Phys. **118**, 364 (2003).
[8] J. P. Devlin and V. Buch, J. Phys. Chem. **99**, 16534 (1995).
[9] N. J. Sack and R. A. Baragiola, Phys. Rev. B **48**, 9973 (1993).
[10] O. S. Heavens, *Optical Properties of Thin Solid Films* (Dover, New York, 1991).
[11] A. H. Narten, C. G. Venkatesh, and S. A. Rice, J. Chem. Phys. **64**, 1106 (1976).
[12] V. Buch and J. P. Devlin, J. Chem. Phys. **94**, 4091 (1991); B. Rowland, N. S. Kadagathur, J. P. Devlin, V. Buch, T. Feldman, and M. J. Wojcik, J. Chem. Phys. **102**, 8328 (1995).
[13] N. Horimoto, H. S. Kato, and M. Kawai, J. Chem. Phys. **116**, 4375 (2002); B. Rowland, M. Fisher, and J. P. Devlin, J. Chem. Phys. **95**, 1378 (1991).
[14] U. Raut, B. D. Teolis, M. J. Loeffler, R. A. Vidal, M. Fama, and R. A. Baragiola, J. Chem. Phys. **126**, 244511 (2007).
[15] F. Rouquerol, J. Rouquerol, and K. Sing, *Adsorption by Powders & Porous Solids: Principles, Methodology and Applications* (Academic, San Diego, 1999).
[16] J. Rouquerol, D. Avnir, C. W. Fairbridge, D. H. Everett, J. H. Haynes, N. Pernicone, J. D. F. Ramsay, K. S. W. Sing, and K. K. Unger, Pure Appl. Chem. **66**, 1739 (1994).
[17] S. J. Gregg and K. S. W. Sing, *Adsorption, Surface Area, and Porosity*, 2nd ed. (Academic, London, 1982).
[18] J. V. Martonchik and G. S. Orton, Appl. Opt. **33**, 8306 (1994).
[19] G. A. Kimmel, K. P. Stevenson, Z. Dohnalek, R. S. Smith, and B. D. Kay, J. Chem. Phys. **114**, 5284 (2001); G. A. Kimmel, Z. Dohnalek, K. P. Stevenson, R. S. Smith, and B. D. Kay, J. Chem. Phys. **114**, 5295 (2001).
[20] W. Hagen, A. Tielens, and J. M. Greenberg, Chem. Phys. **56**, 367 (1981).
[21] W. M. Grundy and B. Schmitt, J. Geophys. Res. **103**, 25809 (1998).
[22] J. Tóth, *Adsorption: Theory, Modeling, and Analysis* (Marcel Dekker, New York, 2002).
[23] D. M. Butler, G. B. Huff, R. W. Toth, and G. A. Stewart, Phys. Rev. Lett. **35**, 1718 (1975).
[24] N. D. Hutson and R. T. Yang, Adsorption **3**, 189 (1997); V. K. Dobruskin, Langmuir **14**, 3840 (1998).
[25] W. Rudzinksi and D. H. Everett, *Adsorption of Gases on Heterogeneous Surfaces* (Academic, New York, 1992).
[26] L. Chaix and F. Domine, J. Phys. Chem. B **101**, 6105 (1997).
[27] G. Mulas, G. A. Baratta, M. E. Palumbo, and G. Strazzulla, Astron. Astrophys. **333**, 1025 (1998).